PHYSICAL REVIEW B **76**, 195437 (2007)

Resputtering phenomena and determination of composition in codeposited films

J. M. Gregoire
Department of Physics, and Cornell Fuel Cell Institute, Cornell University, Ithaca, New York 14853, USA

M. B. Lobovsky and M. F. Heinz
Department of Applied and Engineering Physics, Cornell University, Ithaca, New York 14853, USA

F. J. DiSalvo
Department of Chemistry and Chemical Biology, and Cornell Fuel Cell Institute, Cornell University, Ithaca, New York 14853, USA

R. B. van Dover
Department of Materials Science and Engineering, and Cornell Fuel Cell Institute, Cornell University, Ithaca, New York 14853, USA
(Received 13 June 2007; published 26 November 2007)

The use of standard characterization techniques to determine elemental compositions in composition spread thin films is time intensive. Combinatorial, high-throughput studies of thin film materials demand high-throughput determination of film composition. We discuss the possibility of calculating codeposited film compositions from deposition profiles obtained during single-source sputtering. In the context of dc magnetron sputtering, we find that while this technique is appropriate for the Pd,Pt,Ti system, it yields atomic ratios in a Pt,Pb composition spread thin film that vary significantly from values measured with wavelength-dispersive x-ray spectroscopy. A model for resputtering during codeposition is presented to account for these discrepancies and the model is used to calculate resputter rates during Pt,Pb codeposition. We also employ our model to estimate the resputtering susceptibility of commonly sputtered elements.

DOI: 10.1103/PhysRevB.76.195437 PACS number(s): 81.15.Aa

I. INTRODUCTION

The synthesis of combinatorial libraries of inorganic materials is an increasingly popular technique employed in materials optimization and discovery. Deposition of thin film composition spreads from multiple sources is an attractive technique for creating such libraries as it allows for fabrication of the libraries in a high-throughput regime.[1,2] We discuss the ability to determine elemental compositions in the thin film while minimizing the use of traditional characterization techniques that compromise the high-throughput nature of the study. Our discussion is carried out in the context of magnetron sputtering, which is an attractive deposition technique in combinatorial studies as it offers constant, comparable deposition rates for many elements.[2]

The deposition of the composition spread thin films can be performed by sequential[3] or simultaneous[2] deposition of the constituents. Given deposition rates and profiles for the constituents, the elemental composition of a film sputtered in sequential layers can be easily calculated provided that the individual layers are sufficiently thick. The thickness of each layer must be large enough that the deposition of a layer does not significantly alter the just-deposited layer. With decreasing layer thickness and in the ultimate limit of simultaneous deposition (codeposition), interactions among the deposited material and projectiles from the deposition sources may cause the stoichiometry of the film to differ from that which is calculated using deposition rates from individual sources. We note that the codeposition regime is desirable as it yields films that are intimately mixed in the as-deposited state.

The said interactions will differ with deposition technique (PLD, CVD, etc.). Chemical interactions among the deposited species will be relatively independent of deposition technique while interactions such as the removal of film material by bombarding species will be negligible for evaporated films but may be significant for deposition techniques involving higher energy species. The current work discusses such interactions in the case of codeposition from single-element targets using DC magnetron sputtering in an inert atmosphere and we note that the phenomena discussed are of equal interest for the case of ion beam sputtering.

A. Resputtering

In the deposition scenario at hand, an inert gas ion (e.g., Ar^+) is accelerated across the cathode dark space and bombards a biased metal target (cathode). The collision may eject target atoms, and with some probability the inert gas atom reflects as an energetic neutral atom. Positively charged ions that reflect from the target are decelerated across the cathode dark space and thus do not contribute to resputtering. The net result is a flux of target atoms and reflected gas atoms impinging the substrate. We are interested in the arrival rate and energy of each species at the substrate as well as the accumulation rate of the deposited (metal) species during both single-source and multisource sputtering. Table I gives the symbols used for these molar rates. Subscripts of these symbols will indicate the species whose rate is being referenced. All values of ${}^aR$ for species from a given source are assumed to be independent of the operation of other sources.

During deposition from a single source, the deposited metal is partially resputtered from the substrate by reflected gas neutrals and self-sputtering. These phenomena, collectively referred to as *intrinsic resputtering*, result in a positive intrinsic resputtering fraction $({}^aR-{}^sR)/{}^aR$.

 ©2007 The American Physical Society

TABLE I. Symbols used for the various molar rates at a given point on the substrate and for given sputtering parameters.

Symbol	Molar rate
${}^{a}R$	Arrival at substrate
${}^{s}R$	Accumulation during single-source sputtering
${}^{c}R$	Accumulation during cosputtering
${}^{c}r$	Effective resputter rate due to phenomena unique to cosputtering

Hoffman[4] asserted that, in the absence of projectile scattering with a background gas, this fraction is well parametrized by the target-projectile atomic mass parameter,

$$\mu = \frac{M_{\text{target}} - M_{\text{projectile}}}{M_{\text{target}} + M_{\text{projectile}}}. \quad (1)$$

He mapped this parametrization with thirty measurements of intrinsic resputtering for a particular geometry in an ion beam deposition system. For the sputtering of Pt by 1 keV Ar, the intrinsic resputtering was measured to be about 16% of the Pt arrival rate: 12% from resputtering by reflected Ar and 4% from Pt self-sputtering. Since, for example, the mass parameter μ for Pb sputtered by Ar is roughly equivalent to that of Pt by Ar, the intrinsic resputtering fractions should be approximately the same.

In addition to this intrinsic resputtering, when targets are powered simultaneously, one depositing species can be resputtered by the other depositing species or by Ar neutrals reflected off the other target(s). Also, resputter rates from intrinsic phenomena may be significantly altered by the coexistence of multiple species on the growing film's surface. These phenomena do not occur in single-source deposition and result in cosputter accumulation rates ${}^{c}R = {}^{s}R - {}^{c}r$.

Limited control of resputtering can be achieved by use of ion sources (ion-assisted deposition) and substrate bias (especially in reactive sputtering). We do not discuss such techniques as we are interested in the codeposition analogue of intrinsic resputtering. We do, however, note that these techniques have spawned studies of resputtering of multicomponent films, such as the measuremenets and models of Harper and Gambino.[5]

Resputtering from growing multicomponent films has also been previously studied in the context of deposition from a single alloy target.[6–11] Eisenmenger-Sittner *et al.* and Bauer *et al.*[6,7] studied resputtering effects of Cu and Pb sputtered from a single target with low Pb loading. They simulate six resputter phenomena: Ar, Cu, and Pb each impinging on Cu and on Pb. This work and that of Shah and Carcia,[9] which addresses resputtering in the ion beam sputtering of an alloy target, are of particular interest as they note variations in resputtering with differing substrate position (relative to the target).

Bruce *et al.*[12] studied resputtering in the sequential deposition of W and Si from separate magnetron sources. Their sputter geometry involves substrate movement such that each source deposits in the standard planar face-to-face geometry. They find that as the sequentially deposited layers become increasingly thin, the resputtering of the just-deposited layer by the next layer's source results in measurably different bulk compositions. Similar resputtering effects have been observed in pulsed laser deposition from a multicomponent target, which is well described as the sequential deposition of thin layers. Resputtering in this context are observed and modelled by Sturm and Krebs.[10]

Resputtering in the codeposition of Ti and W has been modelled with TRIM calculations by Bergstrom *et al.*[13] Their simulations revealed that the primary cause of resputtering is energetic Ar reflected from the W target, a result that is in agreement with the present work.

In multisource sputtering, inert gas atoms reflected from different sources must be treated as different projectiles as their energy distributions will depend on the target material and cathode voltage. Thus, with codeposition from n single element sources, n species accumulate on the substrate with $2n^2$ resputtering phenomena occurring at the growing film's surface. While intrinsic resputtering occurs at a film surface with unity surface concentration, the film surface in cosputtering has a finite concentration of all n elements. Thus cosputtered films will never have compositions equal to those calculated from single source accumulation rates. We demonstrate that the differences are negligible in some instances while significant in others.

II. MEASUREMENTS OF FILM COMPOSITION AND DEPOSITION RATES

A. EDS and WDS measurements

Energy dispersive x-ray spectroscopy (EDS) analysis of a ternary Pd,Pt,Ti composition spread was performed using a JEOL 8900 EPMA Microprobe. Quantization of elemental concentrations were calculated with NORAN System SIX software using the Pd L, Pt L, and Ti K x-ray counts.

Wavelength-dispersive x-ray spectroscopy (WDS) analysis of Pt,Pb binary composition spreads were performed using the same instrument. PbS and Pt polycrystalline bulk samples were used as standards, and M_{α} x-rays were counted after diffraction through a TAP crystal. The raw data was then corrected for absorption and thin film effects using GMRFilm,[14] providing Pb:Pt atomic ratios used for analysis.

These standards and GMRFilm were also used to measure the thickness of pure element thickness spread films by exploiting the dependence of x-ray counts on film thickness.

B. *In situ* measurements of single source deposition profiles

The deposition system, described previously,[15] contains a crystal deposition monitor which can be moved across the deposition region, measuring mass accumulation rates at different positions. The corresponding ${}^{s}R$ values are fit to an empirical function for the deposition rate from the given source as a function of substrate position. To establish the validity of this method, fitted profiles were compared to film

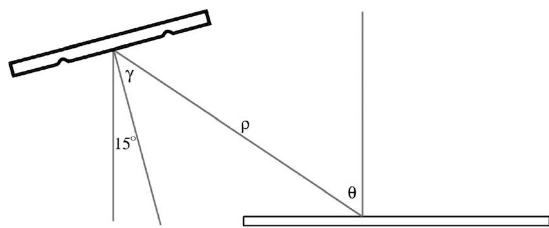

FIG. 1. Relative position of the 3 in. substrate (bottom) and one of the 2 in. targets (upper left) in the deposition system is shown. The important geometrical variables for a given point on the substrate are noted. The figure is drawn approximately to scale.

thickness measurements performed on a thickness spread thin film using WDS. The crystal monitor data and fitting routines were found to produce the WDS thickness values to within a few percent.

III. DEPOSITION GEOMETRY

Composition spread films are sputtered from two or three sources positioned such that the targets are centered 8.3 cm from substrate center, 4.2 cm out of the substrate plane and also confocally tilted 15° from substrate parallel (Fig. 1). While the majority of sputtered material is ejected from the ring whose cross section is drawn on the target, we approximate that atoms leave the target at an angle γ, travel a distance ρ to a substrate point and impinge at an angle $\theta=\gamma+15°$ from substrate normal.

IV. HIGH-THROUGHPUT DETERMINATION OF COMPOSITIONS IN A Pd,Pt,Ti COMPOSITION SPREAD THIN FILM

A Pd,Pt,Ti ternary composition spread was deposited on a 3 in. Si wafer. The single thin film covers approximately the central half of the ternary composition space; that is, the three elemental concentrations each vary from approximately 10% to 80%. The elemental concentrations were measured by EDS at 27 substrate positions and compared to those inferred from single-source profiles (Sec. II B).

At a given substrate position, the normalized atomic ratios Pd:Pt:Ti$=a:b:c$ are described by

$$c = 1 - a - b, \quad a \in \{0,1\}, \quad b \in \{0,1-a\}. \tag{2}$$

A reasonable quantification of the difference between two normalized ternary atomic ratios $a_1:b_1:c_1$ and $a_2:b_2:c_2$ is the distance between the two points in the partial plane described by Eq. (2)

$$[(a_1 - a_2)^2 + (b_1 - b_2)^2 + (c_1 - c_2)^2]^{1/2}. \tag{3}$$

For standardless EDS measurements of the absolute ratios, 10% is a reasonable value for this quantity. Figure 2 shows that the above techniques for crystal monitor-based profiling of the ternary composition spread produces the EDS values to within the absolute accuracy of the measurement.

The only significant deviations between inferred and measured compositions occur for the lowest Pd concentrations,

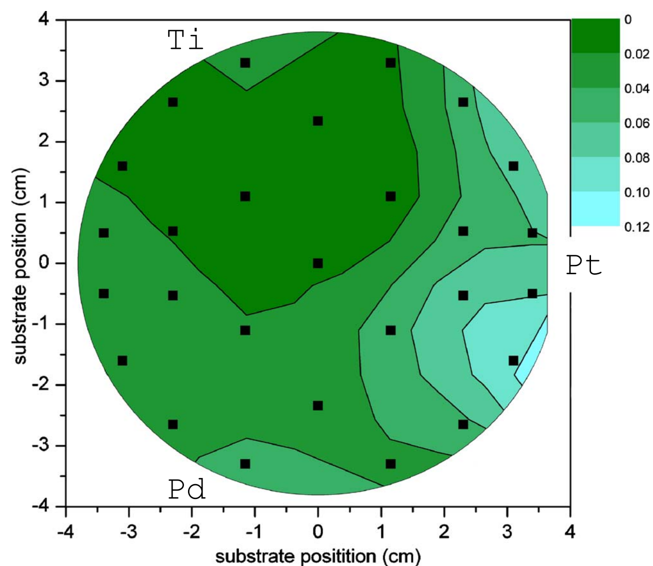

FIG. 2. (Color online) For the Pd,Pt,Ti composition spread, the error [Eq. (3)] in determining EDS-measured film compositions using crystal monitor data is interpolated across the substrate. The orientation of the three targets is noted by the element symbols and the substrate positions of the EDS measurements are plotted.

where crystal monitor data provides a higher Pd concentration than EDS detects. Regardless of absolute compositions, EDS measurements of relative changes in elemental concentrations are accurate to an atomic percent. Thus our comparison of crystal monitor and EDS compositions suggest a systematic, preferential decrease in the accumulation of Pd near the Pt source. In the following section we explore this phenomenon quantitatively for a two element system in which the effect is more pronounced.

V. RESPUTTERING PHENOMENA IN THE CODEPOSITION OF Pb AND Pt

A. Film deposition

Thin film composition spreads containing Pt and Pb were deposited onto one substrate held at 60 °C and one held at 200 °C. Depositions were carried out in 5 mT Ar with Pt and Pb target potentials −370 and −320 V with respect to chamber ground. The molar deposition rate at substrate center from each target was measured before film deposition with the crystal monitor; the individual rates were measured again after film deposition and found to be unchanged, demonstrating the stability of the sputter sources. These rates for Pt and Pb were 2.0 and 2.3 nmoles/s/cm^2, respectively. Given these rates and measured deposition profiles, the Pb:Pt ratio inferred from crystal monitor data is given in Fig. 3. A film with this composition profile could be made by sequential deposition of sufficiently thick layers, as discussed in Sec. I.

B. Model for calculation of resputtering rates

Given relations among the rates in Table I, single-source deposition profiles can be used to calculate resputtering rates

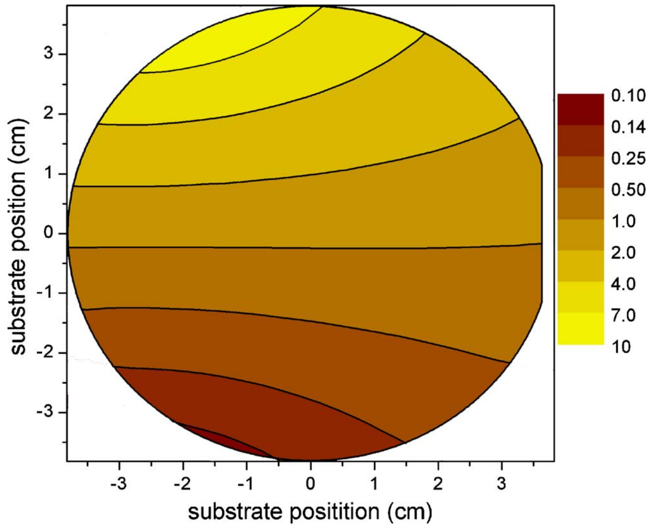

FIG. 3. (Color online) Map of atomic ratio Pb:Pt for the binary composition spread is inferred from crystal monitor profiles.

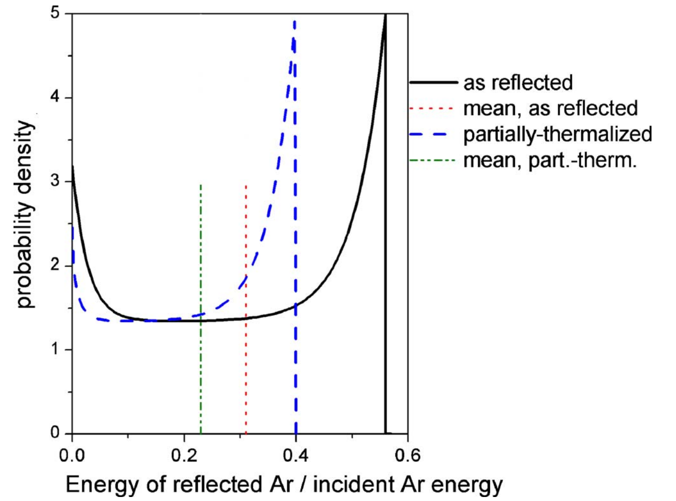

FIG. 4. (Color online) Probability density function of reflected Ar energy is plotted both at the surface of the target responsible for reflection and 5.3 cm from the target, where the Ar has been partially thermalized by collisions with the background 5 mT Ar. The mean energies of the two distributions are also noted.

and thus compositions of cosputtered films. In this section, we develop a model of resputtering in the Pb,Pt system which provides such relations. While the accumulation of Ar in the growing film is neglected (${}^{s}R_{\mathrm{Ar}}={}^{c}R_{\mathrm{Ar}}=0$), the arrival rates of reflected Ar neutrals, ${}^{a}R_{\text{Ar-Pt}}$ and ${}^{a}R_{\text{Ar-Pt}}$ are included, where the hyphenation indicates the target responsible for Ar reflection. As presented in Sec. II B, the crystal monitor accurately measures ${}^{s}R$. The atomic ratios Pb:Pt measured by WDS are ${}^{c}R_{\mathrm{Pb}}/{}^{c}R_{\mathrm{Pt}}$.

Define ${}^{s}\chi$ to be the bulk atomic ratio Pb:Pt for a film sputtered sequentially from the two targets (Fig. 3). Define ${}^{c}\chi$ to be this ratio for a codeposited film,

$$ {}^{c}\chi = \frac{{}^{s}R_{\mathrm{Pb}} - {}^{c}r_{\mathrm{Pb}}}{{}^{s}R_{\mathrm{Pt}} - {}^{c}r_{\mathrm{Pt}}}. \tag{4} $$

The error of cosputtered compositions inferred from single-source profiles is meaningfully quantified by the fractional deviation from the true cosputtered ratio,

$$ \frac{{}^{s}\chi - {}^{c}\chi}{{}^{s}\chi}. \tag{5} $$

1. Reflection of Ar neutrals

The dynamics of reflection of Ar neutrals are not calculated here but are extracted from semiquantitative data in Ref. 7, which includes analysis of the dc sputtering of a Pb target with 500 V applied. This work presents results of TRIM calculations of the fraction of Ar reflected from the Pb target and the energy spectrum of the reflected Ar as a function of reflection angle. For a given scattering angle within the scope of our substrate (see Fig. 1), the energy profile (in units of the bombarding Ar energy) is approximately given by Fig. 4. This scaled energy profile is used for Ar reflected from both Pb and Pt targets. The assumption that the energy spectrum from a Pt target will be similar to that of a Pb target follows from the argument that reflection energetics are similar for any target with mass much greater than the inert projectile.[16]

In the absence of scattering with a background gas, the ratio of energetic Ar departing the target at an angle γ to that of Pb ejected into γ is equal to the ratio of arrival rates at a corresponding substrate position,

$$ {}^{a}R_{\mathrm{Ar-Pb}} = \beta_{\mathrm{Pb}}{}^{a}R_{\mathrm{Pb}}. \tag{6} $$

The simulation of Bauer et al.[7] provides a total reflected Ar to sputtered Pb ratio (averaged over angles γ) of 0.247. While this value certainly varies with ejection direction γ, we invoke an isotropic approximation, using Eq. (6) with $\beta_{\mathrm{Pb}}=0.247$. We note that comparison of the semiquantitative data for the Ar flux[7] and our measured Pb flux as functions of γ indicate that this approximation is reasonable for $25° < \gamma < 55°$, the approximate range that encloses our substrate. Despite the difference in sputtering voltage, we assume that this value and the appropriately scaled distribution of Fig. 4 sufficiently describe Ar reflection from our Pb target.

Simulations performed by Eckstein and Biersack[16] suggest that the reduced energy [Eq. (15)] and mass ratio parametrize both the probability for energetic reflection of incident Ar and the fraction of energy retained upon reflection. Their work indicates that the change in these parameters from our sputtering of Pt to that of Pb results in changes in the reflection probability and fraction of reflected energy that are less than 10%. Ignoring these small changes, since the sputter yield of Pt by Ar is a factor of 3.3 lower than Pb by Ar for the relevant operating voltages, the arrival rate of Ar at the Pt target must be higher than at the Pb target by this factor to remove an equal number of target atoms. We thus approximate $\beta_{\mathrm{Pt}}=3.3\beta_{\mathrm{Pb}}$ and

$$ {}^{a}R_{\mathrm{Ar-Pt}} = \beta_{\mathrm{Pt}}{}^{a}R_{\mathrm{Pt}}. \tag{7} $$

2. Energy spectra of sputtered Pb and Pt

The energy spectra of sputtered Pb and Pt (as they leave their respective targets) are assumed to be well described by the semiempirical energy distributions set forth in Ref. 17. With Ar impinging at energy E_{Ar}, the probability density function for the energy E of sputtered atoms is proportional to

$$\left[1-\left(\frac{E_b+E}{mE_{\mathrm{Ar}}}\right)^{1/2}\right]\Bigg/\left[E^2+\left(1+\frac{E_b}{E}\right)^3\right], \tag{8}$$

where m is the energy transfer factor from collision theory and E_b is the binding energy of the sputtered materials. While the validity of this equation has not been extensively verified for Pb and Pt sputtered by Ar, it yields a most probable energy 3.8 eV for Pt sputtered by 370 eV Ar, which is a reasonable value given measured data in Ref. 18. For comparison, the most probable energy for Pb sputtered by 320 eV Ar is 2.2 eV.

The distribution of Eq. (8) allows for finite probability density at arbitrarily large E. We use a cutoff energy[7]

$$E_{\max}=mE_{\mathrm{Ar}}-E_b, \tag{9}$$

the maximum energy that could be transferred to a sputtered atom by an impinging atom according to linear cascade theory.

3. Thermalization of sputtered material and reflected Ar

As sputtered Pb and Pt atoms and reflected Ar travel from the targets to the substrate, collisions with the background Ar gas cause thermalization of these superthermal species. This phenomenon has been treated by Monte Carlo simulations[19] that model collisions by picking the energy loss of the energetic atom and the scattering angle from appropriate distributions. For ease in calculation, we use the continuous energy loss model for gas phase scattering.[20] This model includes an energy loss per distance traveled that is proportional to the projectile velocity. Treating thermalization as the zero-point of projectile energy, the energy of a projectile a distance ρ away from the target is

$$E=(1-\rho/\rho_{\max})^2E_0, \tag{10}$$

where E_0 is the energy of the projectile leaving the target and $\rho_{\max}$ is the distance traveled by the projectile before thermalization,

$$\rho_{\max}=AE_0^{1/2}. \tag{11}$$

For a given temperature T in K, Ar pressure p in Pa and Ar to projectile mass number ratio M,

$$A=0.012\left(\frac{1+1/M}{M_{\mathrm{Ar}}}\right)(1+M^{2/3})^{3/4}\frac{T}{p}\frac{\mathrm{cm}}{\mathrm{eV}^{1/2}}. \tag{12}$$

The scattering angles of Pb and Pt, which are much more massive than the thermal constituents (Ar), will be small. Thus, the continuous energy loss approximation, which neglects scattering angles, is reasonably applied to Pt and Pb. While the neglect of scattering angle is less appropriate for the thermalization of energetic Ar, the mean free path of Ar in our system is greater than the target-substrate distance. The implications of these approximations for the results of the following calculations are discussed in Sec. VII B.

The convolution of the above energy profiles, Eq. (8) and Fig. 4, with Eq. (10) provides the energy distribution for the projectiles, $\Xi(E,\rho)$, where ρ is the distance from the appropriate target (see Fig. 1). This distribution has a maximum energy $E_{\max}(\rho)$ easily calculated with Eqs. (9) and (10). It is worth noting that convolution of a probability distribution with Eq. (10) does not preserve probability. The continuous energy loss model mandates that at nonvanishing ρ, some fraction of the projectile population has thermalized, and thus, the distribution describes only the fraction that remains energetic. Or equivalently, the full energy distribution is taken to be an energetic fraction

$$\int_0^{E_{\max}(\rho)}\Xi(E,\rho)dE_B \tag{13}$$

and the (remaining) thermalized fraction that diffuses in the 5 mT Ar atmosphere.

Figure 4 shows the evolution of the reflected Ar energy profile after thermalizing through 5.3 cm travel from the target. At this point 29% of reflected Ar have thermalized and the remaining 71% have a mean energy significantly lower than the mean energy at $\rho=0$.

4. Sputter yields at the substrate

For the eight sputter yields of interest, we use the semiempirical model set forth by Matsunami *et al.*[21,22] and recently discussed by Seah *et al.*[23] For an atom A with binding energy E_b, the threshold energy $E_{t,AB}$ for sputtering by projectile species B is

$$E_{t,AB}=E_b[0.08+0.164(M_A/M_B)^{0.4}+0.0145(M_A/M_B)^{1.29}]. \tag{14}$$

The reduced energy ϵ for a collision by a projectile with energy E is given by

$$\epsilon=\frac{0.03255}{Z_AZ_B(Z_A^{2/3}+Z_B^{2/3})^{1/2}}\frac{M_A}{M_A+M_B}E. \tag{15}$$

For the A-B combinations of interest, the sputter yield Y is given by

$$Y_{AB}\propto\frac{1}{E_{b,A}}\left[1-\left(\frac{E_{t,AB}}{E}\right)^{1/2}\right]^{2.8}, \tag{16}$$

where the proportionality constant is a function of the reduced energy, elemental properties of A and B, and empirically determined coefficients. The proportionality constants used in this study were taken from Ref. 24.

5. Angle of substrate incidence

The above sputter yields [Eq. (16)] assume normal incidence. Neglecting changes in trajectory due to gas phase scattering, the angle of impact at a given substrate position is θ as drawn in Fig. 1. While no data concerning the angular variation in sputter yields with Pb or Pt projectiles could be

found in the literature, for Ar impinging on metal surfaces with $\theta < 60°$, the yield has been shown to vary as $(\cos\theta)^{-1}$.[25] This functional form for angular dependence is used for all sputter yields.

6. Effective sputter yield and resputter rates

While the yield of a projectile with known energy is given by Eq. (16), the average yield of a projectile with energy distribution Ξ at substrate position (ρ,θ) is

$$\Upsilon_{AB}(\rho,\theta) = \int_{E_{t,AB}}^{E_{\max}(\rho)} Y_{AB}(E)\Xi(E,\rho)(\cos\theta)^{-1}dE. \quad (17)$$

Then the arrival rate of X (X=Pt or Pb) is given by

$$^{a}R_X = {}^{s}R_X(1-\Upsilon_{XX}-\beta_X\Upsilon_{X\mathrm{Ar}-X})^{-1}. \quad (18)$$

Using this equation, the molar rates determined by crystal monitor measurements are adjusted for intrinsic resputtering to provide arrival rates of Pt and Pb. Arrival rates for reflected Ar can then be obtained with [Eqs. (6) and (7)].

7. Surface concentration

The resputter rate of a given species at the substrate will be proportional to the probability P_X that an approaching projectile will impinge on that species. We approximate that the cross section for collision of the (low energy) projectiles and a Pt,Pb alloy monolayer is sufficiently high that sputtering of the Pt,Pb film occurs only from the first monolayer. The relative cross section for collision with X in the first monolayer will be proportional to the concentration of X in that layer. Given the similar masses and atomic radii of Pb and Pt, we approximate the proportionality constant to be unity.

As alluded to in Sec. I A, the surface concentrations of deposited species are not unity during codeposition. Neglecting the reflection of (low energy) Pb and Pt from the substrate surface, as a gas-phase metal atom approaches the substrate, the probability P that it is a Pb atom is

$$^{a}P_{\mathrm{Pb}} = \frac{^{a}R_{\mathrm{Pb}}}{^{a}R_{\mathrm{Pb}} + {}^{a}R_{\mathrm{Pt}}}. \quad (19)$$

This atom becomes a surface atom and remains so until it is covered by the next monolayer of material, at which point, in our approximation, it can no longer be resputtered. At this time, the probability that it is a Pb atom is given by

$$^{c}P_{\mathrm{Pb}} = \frac{^{c}R_{\mathrm{Pb}}}{^{c}R_{\mathrm{Pb}} + {}^{c}R_{\mathrm{Pt}}}. \quad (20)$$

If the accessibility of the atom to projectiles is constant over the time spent as a surface atom, the time-averaged probability of a given projectile impinging on Pb and Pt are

$$P_{\mathrm{Pb}} = ({}^{a}P_{\mathrm{Pb}} + {}^{c}P_{\mathrm{Pb}})/2, \quad P_{\mathrm{Pt}} = 1 - P_{\mathrm{Pb}}. \quad (21)$$

8. Cosputtering resputter rates

The resputter rate of X from a given projectile is the product of P_X [Eq. (21)], the effective yield of the projectile [Eq. (17)], and the arrival rate of the projectile [Eqs. (6), (7), and (18)]. The absolute resputter rate of X is the sum of the sputter rates from each projectile:

$$^{a}R_X - {}^{c}R_X = P_X\sum, \quad \text{with} \sum = \sum_B \Upsilon_{XB}{}^{a}R_B. \quad (22)$$

For X=Pb, the solution is

$$2{}^{c}R_{\mathrm{Pb}} = {}^{a}R_{\mathrm{Pb}} - {}^{c}R_{\mathrm{Pt}} - (1+{}^{a}P_{\mathrm{Pb}})\sum + \left\{\left[{}^{c}R_{\mathrm{Pt}} - {}^{a}R_{\mathrm{Pb}} + (1+{}^{a}P_{\mathrm{Pb}})\sum\right]^2 - 4\left({}^{a}P_{\mathrm{Pb}}\sum - {}^{a}R_{\mathrm{Pb}}\right)\right\}^{1/2}. \quad (23)$$

The equation for $^{c}R_{\mathrm{Pt}}$ is given by interchanging the element symbols. This system of equations can be solved in closed form, yielding expressions for the accumulation rates during cosputtering.

C. Results of calculated resputter rates in Pt,Pb codeposition

The calculated cosputter accumulation rates [Eq. (23)] and crystal monitor data are used to calculate the fractional loss in Pb:Pt due to cosputtering [Eq. (5)], yielding the contour plot of Fig. 5(d). For the 21 data points with highest Pb concentration [excluding the bottom row of points in Fig. 5(a)], our simulations produce the WDS measured Pb:Pt values with an average absolute error of 13%, compared to the error of 45% using the raw crystal monitor data. For the six points with crystal monitor Pb:Pt values of 25%, the calculations predict a Pb:Pt value of 12% while the measured value is 6%. That is, the calculations correctly predict that a large fraction of the Pb will be resputtered from the film during codeposition, but the magnitude is not large enough to correctly produce WDS values.

1. Relative yields of different projectiles

The effective yields [Eq. (17)] of the four projectiles on both pure Pb and Pt surfaces are given as a function of substrate position in Fig. 6. Our calculations indicate that the Ar projectiles have far higher yields, but we note that arrival rates are not included in this comparison.

The WDS data of Fig. 5(b) clearly suggests that Pb is being preferentially removed from the substrate in a way that correlates to distance from the Pt source. A question of interest is whether Pt projectiles or Ar reflected from Pt are the cause for this removal. The ratio of the Pb resputter rates of these two projectiles is given in Fig. 7, which shows that Pb resputtering due to Ar reflected from Pt is dominant.

2. Enhancement of accumulation rate due to codeposition

The effective resputter rate due to cosputtering, ^{c}r, can be negative. Suppose the projectiles from the source of element X are the dominant resputter projectiles in codeposition. Due to the reduced probability for projectile collision with X on the growing film's surface (compared to the unity probability of single source deposition), codeposition may result in a higher accumulation rate of X, that is $^{s}R_X < {}^{c}R_X < {}^{a}R_X$. In our Pt,Pb codeposition, the calculations indicate this is the case

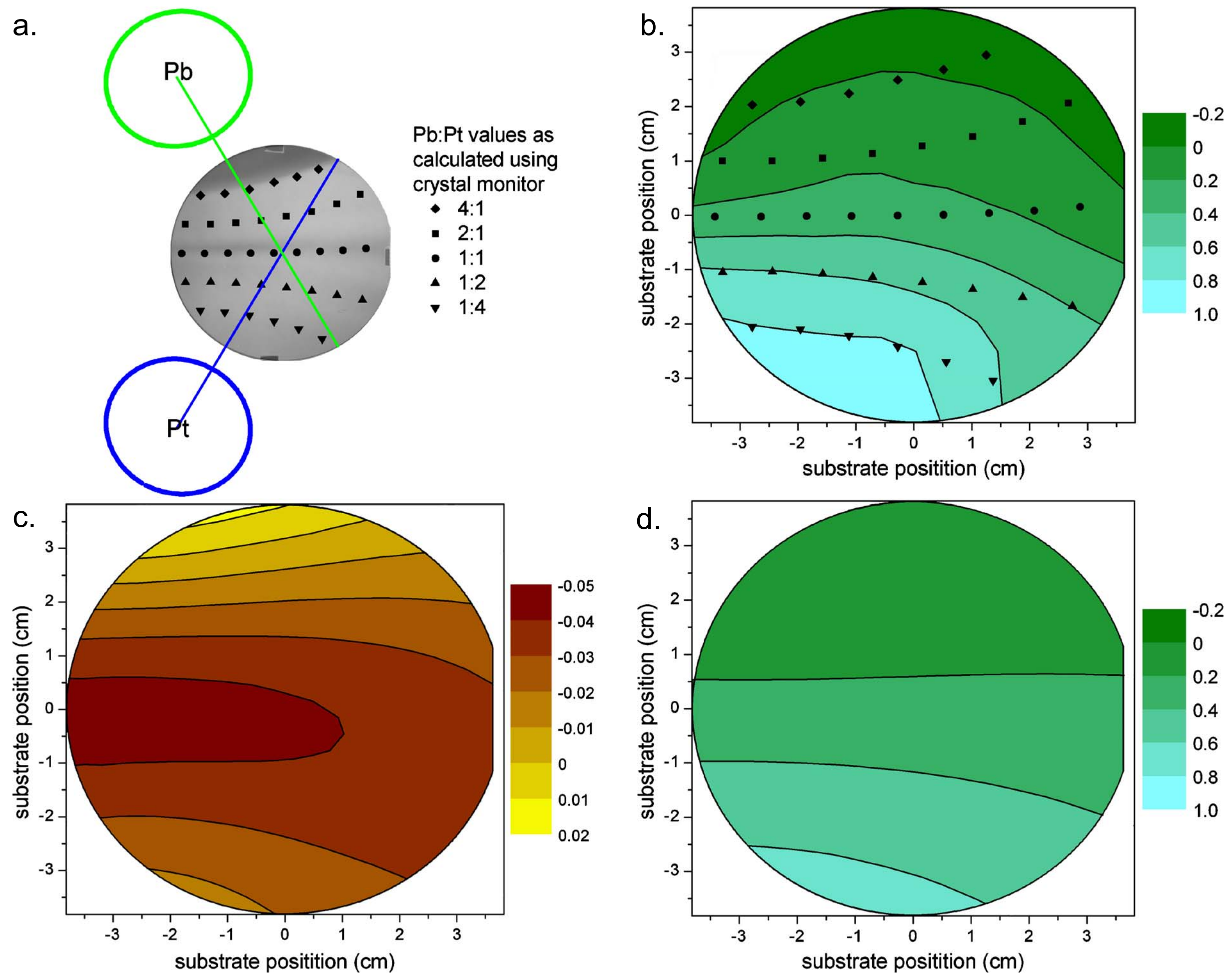

FIG. 5. (Color online) (a) Positions of the 27 WDS measurements on the Pt,Pb composition spread are shown and categorized by the nominal stoichiometries determined from crystal monitor data. The substrate image is a photograph of the sputtered composition spread. Dark regions indicative of surface roughness coincide with compositional contours. The positions of the two 2 in. targets are also shown as well as their axes in the substrate plane. (b) Fractional difference in atomic ratio Pb:Pt between crystal monitor measurements and WDS measurements [Eq. (5)] is plotted in the outline of the substrate. (c) Fraction of Pt single-source accumulation rate that becomes resputter rate due to codeposition is calculated and can be compared with (d). Negative values correspond to cosputter accumulation rates that exceed those of single-source sputtering. (d) Using calculated values of ${}^{c}\chi$ (see Sec. V B), values of Eq. (5) are plotted for comparison with (b).

for Pt over most of the substrate. A contour plot of ${}^{c}r_{\mathrm{Pt}}/{}^{s}R_{\mathrm{Pt}}$ is given in Fig. 5(c).

3. Note on Pb resputter fraction

Figure 5(c) demonstrates that

$$\left|\frac{{}^{c}r_{\mathrm{Pt}}}{{}^{s}R_{\mathrm{Pt}}}\right| \ll 1, \tag{24}$$

i.e., cosputtering with Pb has little effect on the net accumulation of Pt. In this limit, Eq. (5) can be written in an illuminating form,

$$\frac{{}^{s}\chi - {}^{c}\chi}{{}^{s}\chi} = 1 - \frac{1 - {}^{c}r_{\mathrm{Pb}}/{}^{s}R_{\mathrm{Pb}}}{1 - {}^{c}r_{\mathrm{Pt}}/{}^{s}R_{\mathrm{Pt}}} \approx \frac{{}^{c}r_{\mathrm{Pb}}}{{}^{s}R_{\mathrm{Pb}}}. \tag{25}$$

That is, ignoring the changes in the resputtering of Pt due to cosputtering, Figs. 5(b) and 5(d) give values of the fraction of single-source Pb accumulation that is resputtered due to codeposition. Figures 5(c) and 5(d) can thus be compared to demonstrate the extent to which the magnitude of codeposition-specific resputtering of Pb exceeds that of Pt.

4. Temperature dependence of resputtering phenomena in codeposition

Figure 8 indicates that increasing the substrate temperature from 60 °C to 200 °C results in negligible differences in resputtering phenomena over most of the substrate. The measured differences do not monotonically correlate with the arrival rate of any of the projectle species in our model. We note that a modification of our model to explain higher temperature depositions may be necessary, especially for Pb-rich film compositions. While we do not offer an alteration to the model here, we suggest that the cause for a temperature dependence in this temperature range is due to an increase in the probability of surface Pb atoms to have an appreciable thermal energy (vis a vis the threshold for sputtering) as

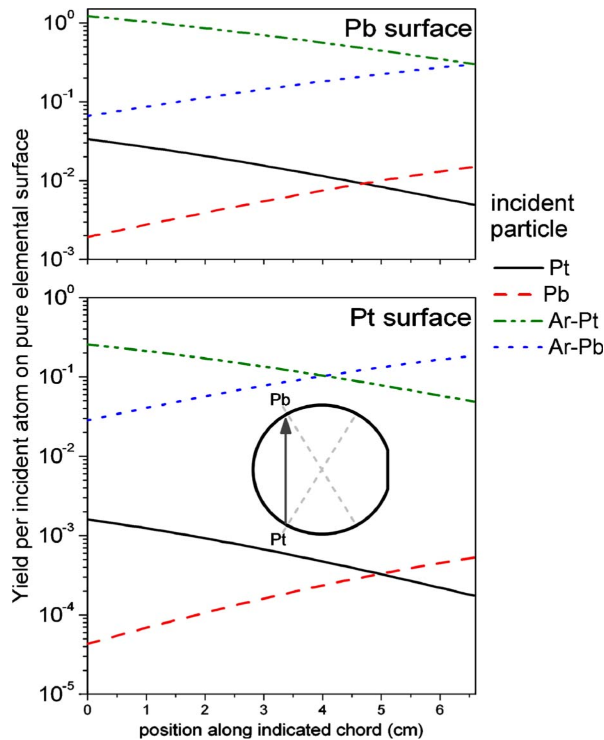

FIG. 6. (Color online) Effective yields [Eq. (17)] for the four projectiles in Pt,Pb codeposition are shown for both pure Pb and pure Pt surfaces. The yields are plotted as a function of position on the substrate line connecting the point closest to the Pt target and point closest to the Pb target. The inset gives a graphical representation of this line.

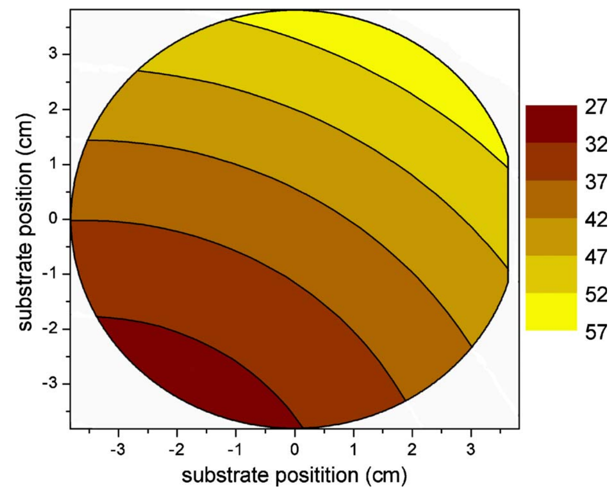

FIG. 7. (Color online) Ratio of the resputter rate of Pb by Ar-Pt during the Pt,Pb codeposition to that of Pb by Pt is plotted across the substrate, demonstrating that Ar-Pt is the projectile more responsible for Pb depletion in the film.

governed by Boltzman statistics. That is, as the rate of spontaneous desorption (evaporation) becomes significant, even low energy projectiles can stimulate desorption (resputtering). While the yields for fcc polycrystalline targets were found to be independent of substrate temperature with ion bombardment in the keV range,[26] the thermal energy effect will be amplified for lower energy projectiles. Further discussion of temperature dependence in resputtering from multicomponent films can be found in Ref. 6, 11, and 13

VI. RESPUTTER YIELD OF Ar REFLECTED FROM Pt FOR 27 ELEMENTS

To illustrate significant parameters in determining the magnitude of resputtering phenomena in codeposition, the total sputter yield $Y_{\text{Ar-Pt},X}$ was calculated for 27 commonly sputtered elements X. The energy spectra, gas scattering, etc. of Sec. V B were used and Eq. (17) was evaluated at substrate center. The results are plotted in Fig. 9 which shows that the heat of sublimation of the elements is a governing factor in determining susceptibility to resputtering. This figure can be used as an indicator of the inability of the crystal monitor (or other single-source sputter profile) data to predict stoichiometry of codeposited films when the deposition includes an element with Ar reflection dynamics similar to those of Pt.

VII. DISCUSSION

A. Pd,Pt,Ti composition spread

The Pd,Pt,Ti system can be treated in the same detail as the Pt,Pb system upon determining an energy spectrum and probability for the reflection of Ar from Pd and Ti targets. The simulations of Eckstein and Biersack[16] can be used to estimate the reflection probability and average reflected energy of Ar from the respective targets. With its lower mass and slightly higher reduced energy for comparable molar deposition rates, the reflection probability of Ar from Pd should be less than 70% and the average reflected energy less than 50% of the values for Pt. Also, the yield of Pd by Ar is higher than the yield of Pt at the respective operating voltages, so the number of Ar impinging the respective targets will be lower for Pd for a given equal (single source) molar deposition rate.

Although the reduced energy [Eq. (15)] required to achieve the desired molar rate from Ti is high due its low sputter yield by Ar, the low Ti to Ar mass ratio results in an estimated Ar reflection probability of 20% of that of Pt and an average absolute reflected energy of 0.1%.

Using the same Pt energy spectrum as above, we calculate the total yields [Eq. (17)] for Pt sputtering Pd and Ti to be $<10^{-3}$ and $<10^{-5}$ across the substrate. The other metal-metal resputtering phenomena in this system are equally insignificant and thus we conclude that for the Pd,Pt,Ti system, the only significant resputtering phenomena are those with Ar-Pt as projectile.

We calculate the total yields for Ar-Pt sputtering Pb to be about three times higher than for Pd and 17 times higher than for Ti and thus conclude that resputtering phenomena associated with cosputtering are far less important for this system compared to the Pt,Pb system, as the EDS and WDS measurements confirm.

In the Pd-rich region (see Fig. 2), the point with the largest deviation [Eq. (3)] is one for which crystal monitor data

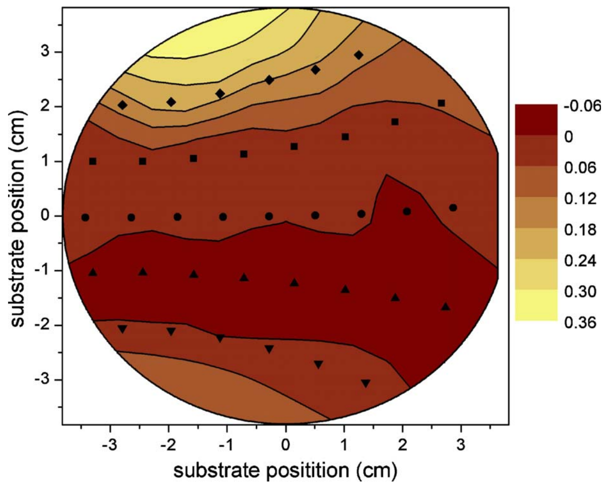

FIG. 8. (Color online) WDS-determined values for Eq. (5) for a Pt,Pb composition spread film deposited on a 200 °C substrate are subtracted by the data in Fig. 5(b) and plotted in the outline of the substrate. The magnitude of this difference is indicative of the importance of increased substrate temperature in codeposited film composition for our Pt,Pb system. The negative values correspond to an increase in Pb concentration with elevated substrate temperature but are within the measurement error and reproducibility limits of sputter conditions.

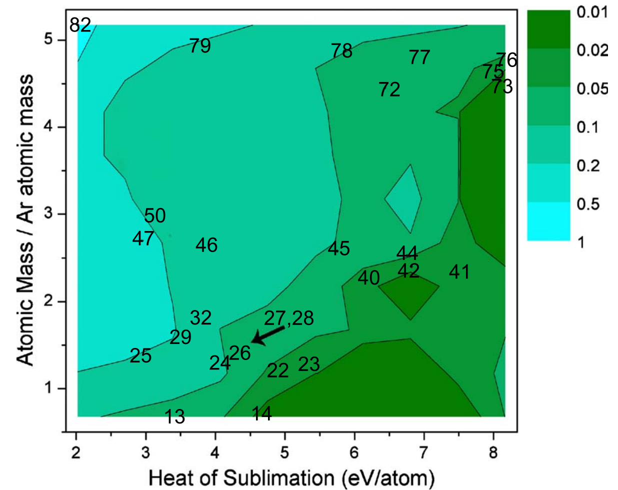

FIG. 9. (Color online) Using the resputtering model of Sec. V B, the effective yield [Eq. (17)] of Ar-Pt impinging the substrate center is plotted in contours as a function of mass ratio and heat of sublimation for 27 commonly sputtered elements. The atomic numbers of the elements are used to identify their approximate positions on the graph.

provides a Pd:Pt:Ti of 10.7:75.6:13.7 while the measured EDS values are 7:80:13. Adjusting crystal monitor data by including Ar-Pt sputtering of Pd with Pd surface sputter probability [Eq. (21)] approximated by crystal monitor Pd concentration gives Pd:Pt:Ti=8.5:77.4:14.0. While the error [Eq. (3)] of the crystal monitor data in producing this EDS measurement is 5.8%, this single adjustment reduces the error to 3.2%. We thus conclude that our model of resputtering phenomena in codeposition reliably describes the observed shortcomings of the determination of film composions using crystal monitor data in the Pd,Pt,Ti system.

B. Implications of resputter model approximations in the Pt,Pb system

As noted in Sec. V B 3, the mean free path for nearly the entire Ar projectile energy spectrum exceeds all target-substrate distances. The application of the continuous energy loss model eliminates the substrate impingement by the highest energy Ar projectiles. These projectiles have significant yields for both Pt and Pb and we expect that as a result, the data in Fig. 6 are an underestimate for the effective Ar resputter yields. We also note that the magnitude of this effect varies with substrate position due to changing target-substrate distance.

Our use of the Thompson model[17] for the energy distribution of atoms ejected from the target neglects any variation with ejection direction. Stuart, Wehner, and Anderson[18,27] found an increase in ejection energy with increasing ejection angle. The simulations of Mahieu *et al.*[28] for Zr sputtered by 400 eV Ar showed that the most probable ejection angles for the highest energy sputtered material are between 35° and 60°, the range of sputtering angles that cover our substrates. An upward shift in Pb and Pt energy distributions would increase the yields from these projectiles. However, the yields would remain much smaller than those of Ar projectiles (see Fig. 6).

The energy spectrum of reflected Ar also changes as a function of angle γ from target normal. The calculations of Bauer *et al.*[7] show that, for large γ, this energy spectrum has a higher density near the maximum energy shown in Fig. 4.

The model for the energy threshold for sputtering [Eq. (14)] assumes normal incidence. Wehner[29] finds that the threshold energy for sputtering decreases with more oblique incidence. While we neglect this θ dependence, it may significantly increase the effective sputter yields for all projectiles by widening the interval of integration in Eq. (17).

While the combination of these approximations may affect the magnitude of resputtering, the collective potential of neglected anisotropies to alter the gradients of resputter rates across the substrate is more significant. Thus the higher density of contour lines in the measured data of Fig. 5(b) compared to the calculated data of Fig. 5(d) is not surprising.

Our final note on approximations is that the absolute sputter yields obtained from[21,24] carry significant yet unquantified uncertainties. Our calculated resputter rates are directly proportional to these yields and thus our calculated results carry these significant uncertainties.

C. Interactions in the growing film

Other phenomena in codeposition that could be important for resputtering are diffusion of species in the film to the film surface as it is deposited and shifts in the binding energy of surface atoms due to atomic interactions in the film. While we do not include these phenomena in the above model, notes on their significance in the Pt,Pb system and in general

codeposition are provided as supplemental information.[30] These notes include discussion of the negative values of Fig. 5(b) and additional resputter calculation data. The role of diffusion has previously been discussed in the context of resputtering.[6,11,13]

D. Applicability to other deposition systems

Since the sputter geometry plays such an important role in resputter phenomena, the absolute resputter rates will vary significantly amongst deposition systems. Our treatment of resputtering and the overall calculated susceptibility to resputtering (Fig. 9) are more system independent.

Beyond deposition geometry, other deposition parameters (e.g., type and pressure of inert gas, target voltages in magnetron sputtering or accelerating voltages in ion beam sputtering) can significantly affect resputtering phenomena. These parameters are included in the model outlined in Sec. V B. Provided availability of a sputter yield for each projectile-film constituent combination [or proportionality constant in Eq. (16)] and initial energy distribution for reflected inert neutrals, this model can be applied to estimate resputtering rates in any codeposition experiment. While the profile used in the present work (Fig. 4) was obtained from TRIM calculations of Ref. 7, targets with different reflection dynamics[16] may require similarly calculated profiles.

VIII. CONCLUSIONS

Single-source profiling can be an effective tool for determining compositions in multigun sputtering. This is particularly useful for high-throughput studies, in which measurements of composition of every location on a composition spread film would be expensive in time and effort. For the codeposition of some sets of elements, modeling film growth as the simple addition of individual rates can lead to significant errors. We have demonstrated that resputtering phenomena account for most of these errors and have developed a model that incorporates the most important effects. While our model includes several approximations which can easily be improved, it provides sufficiently accurate results to demonstrate the primary causes of resputtering in the Pt,Pb system and to provide a framework for determining the importance of these phenomena in other codeposition systems. With the use of this model, compositions can be calculated with an accuracy of a few atomic percent, which is comparable to the best routine absolute composition measurements for thin films.

ACKNOWLEDGMENTS

The WDS analysis was made possible by the Cornell Center for Materials Research Facilities supported by the National Science Foundation under Grant No. DMR-0520404. Primary funding for this work is provided by the Department of Energy, Grant No. DE-FG02-03ER46072.

[1] J. Hanak, J. Mater. Sci. **5**, 964 (1970).
[2] R. B. van Dover, L. F. Schneemeyer, and R. M. Fleming, Nature (London) **392**, 162 (1998).
[3] H. Chang, I. Takeuchi, and X. D. Xiang, Appl. Phys. Lett. **74**, 1165 (1999).
[4] D. W. Hoffman, J. Vac. Sci. Technol. A **8**, 3707 (1990).
[5] J. M. E. Harper and R. J. Gambino, J. Vac. Sci. Technol. **16**, 1901 (1979).
[6] C. Eisenmenger-Sittner, A. Bergauer, and A. Wagendristel, J. Vac. Sci. Technol. A **10**, 3260 (1992).
[7] W. Bauer, G. Betz, H. Bangert, A. Bergauer, and C. Eisenmenger-Sittner, J. Vac. Sci. Technol. A **12**, 3157 (1994).
[8] L. Shaginyan, M. Misina, S. Kadlec, L. Jastrabik, A. Mackova, and V. Perina, J. Vac. Sci. Technol. A **19**, 2554 (2001).
[9] S. I. Shah and P. F. Carcia, J. Vac. Sci. Technol. A **9**, 609 (1991).
[10] K. Sturm and H. U. Krebs, J. Appl. Phys. **90**, 1061 (2001).
[11] J. M. E. Harper, S. Berg, C. Nender, I. V. Katardjiev, and S. Motakef, J. Vac. Sci. Technol. A **10**, 1765 (1992).
[12] R. Bruce, S. Eicher, and W. Westwood, J. Vac. Sci. Technol. A **6**, 1642 (1988).
[13] D. B. Bergstrom, F. Tian, I. Petrov, J. Moser, and J. E. Greene, Appl. Phys. Lett. **67**, 3102 (1995).
[14] R. A. Waldo, M. C. Militello, and S. W. Gaarenstroom, Surf. Interface Anal. **20**, 111 (2004).
[15] J. M. Gregoire, R. B. van Dover, J. Jin, F. J. DiSalvo, and H. D. Abruña, Rev. Sci. Instrum. **78**, 072212 (2007).
[16] W. Eckstein and J. P. Biersack, Z. Phys. B: Condens. Matter **63**, 471 (1986).
[17] M. Thompson, Philos. Mag. **18**, 377 (1968).
[18] R. V. Stuart, G. K. Wehner, and G. S. Anderson, J. Appl. Phys. **40**, 803 (1969).
[19] T. Motohiro and Y. Taga, Surf. Sci. **134**, 494 (1983).
[20] A. Gras-Marti and J. A. Valles-Abarca, J. Appl. Phys. **54**, 1071 (1983).
[21] N. Matsunami, Y. Yamamura, N. Itoh, H. Tawara, and T. Kawamura, Inst. Plasma Phys. Rep. **IPPJ-AM-52**, 37 (1987).
[22] N. Matsunami, Y. Yamamura, Y. Itikawa, N. Itoh, Y. Kazumata, S. Miyagawa, K. Morita, and R. Shimizu, Radiat. Eff. Lett. Sect. **57**, 15 (1980).
[23] M. P. Seah, C. A. Clifford, F. M. Green, and I. S. Gilmore, Surf. Interface Anal. **37**, 444 (2005).
[24] I. W. S. P. Group, www.iap.tuwien.ac.at/www/surface/script/sputteryield (2006).
[25] H. Oechsner, Appl. Phys. **8**, 185 (1975).
[26] C. E. Carlston, G. D. Magnuson, A. Comeaux, and P. Mahadevan, Phys. Rev. **138**, A759 (1965).
[27] R. Stuart and G. Wehner, J. Appl. Phys. **35**, 1819 (1964).
[28] S. Mahieu, G. Buyle, D. Depla, S. Heirwegh, P. Ghekiere, and R. De Gryse, Nucl. Instrum. Methods Phys. Res. B **243**, 313 (2006).
[29] G. Wehner, J. Appl. Phys. **30**, 1762 (1959).
[30] See EPAPS Document No. E-PRBMDO-76-019743 for further discussion of film chemistry and additional figures. For more information on EPAPS, see http://www.aip.org/pubservs/epaps.html